

Electron beam heating effects during environmental scanning electron microscopy imaging of water condensation on superhydrophobic surfaces

K. Rykaczewski,^{1,a)} J. H. J. Scott,¹ and A. G. Fedorov²

¹Material Measurement Laboratory, National Institute of Standards and Technology, Gaithersburg, Maryland 20899, USA

²G.W. Woodruff School of Mechanical Engineering, Georgia Institute of Technology, Atlanta, Georgia 30332, USA

(Received 13 January 2011; accepted 2 February 2011; published online 1 March 2011)

Superhydrophobic surfaces (SHSs) show promise as promoters of dropwise condensation. Droplets with diameters below $\sim 10 \mu\text{m}$ account for the majority of the heat transferred during dropwise condensation but their growth dynamics on SHS have not been systematically studied. Due to the complex topography of the surface environmental scanning electron microscopy is the preferred method for observing the growth dynamics of droplets in this size regime. By studying electron beam heating effects on condensed water droplets we establish a magnification limit below which the heating effects are negligible and use this insight to study the mechanism of individual drop growth. © 2011 American Institute of Physics. [doi:10.1063/1.3560443]

Vapor condensation is an essential part of many technologies in energy generation, automotive engineering, heating, ventilation, and air conditioning, and thermal management. As a consequence, even a moderate improvement in the heat transfer rate during this phase change process could lead to considerable economic savings. Eighty years ago, Schmidt *et al.*¹ demonstrated that the heat transfer rate during dropwise condensation is an order of magnitude higher than during filmwise condensation. Unfortunately, premature degradation of the surfaces and coatings needed for dropwise condensation has prevented the use of this process in practical applications.² Due to their ability to shed water, bio-inspired superhydrophobic surfaces (SHSs) have recently generated a lot of interest and research effort in their application as promoters for dropwise condensation. Several groups have demonstrated that properly designed nanostructured and/or microstructured SHSs can maintain dropwise condensation.^{3–5} Most of the research effort in this area has been focused on the design of the SHSs themselves and characterization of their wetting behavior,^{6,7} and only a few studies have paid attention to the condensation dynamics.^{8–13} All of those studies focused on growth of drops with diameters ranging from $\sim 10 \mu\text{m}$ to a few millimeters. However, imparting nanostructure to the surface results in a significant increase in the number of droplets with diameters below $10 \mu\text{m}$,¹⁴ and those droplets account for the majority of the heat transferred during dropwise condensation.^{15–17} Because the droplets are so small and because the process is dynamic and occurs on complex topography, environmental scanning electron microscopy (ESEM) is the preferred method for imaging in detail the growth of droplets in the sub- $10 \mu\text{m}$ regime. In contrast to other electron beam effects occurring during ESEM imaging such as radiation damage due to water radiolysis,¹⁸ electron beam induced surface wettability modifications,^{19,20} dynamic liquid charging,^{21,22} topographic contrast,²³ and biological sample damage,^{11,24–27} the evaporation of condensed drops has not been systematically studied. In this work, we demonstrate that electron beam can

cause significant heating and fast evaporation of condensed drops during imaging at high magnification necessary for observation drop growth dynamics in the sub- $10 \mu\text{m}$ regime. We characterize the electron beam heating effects by observing the evaporation rates of condensed water droplets under different conditions in the ESEM. Further, we explain the observed experimental trends with a developed model of the process. Lastly, we quantify the ESEM imaging magnification limit below which heating effects are negligible and use this insight to study individual droplet growth during water condensation on randomly stacked cupric hydroxide $[\text{Cu}(\text{OH})_2]$ nanotube-based SHSs.^{28–30}

In this work we quantify the electron beam heating effects by observing behavior of ~ 4 to $\sim 12 \mu\text{m}$ diameter droplets condensed on polished silicon and on $\text{Cu}(\text{OH})_2$ nanotube SHS imaged in viewing areas of $18.6 \times 17.1 \mu\text{m}^2$ and $9.3 \times 8.5 \mu\text{m}^2$ with electron beam energy and current in the 5 keV to 30 keV and 0.019 nA to 2.4 nA range, respectively. Water condensation is achieved by decreasing the sample temperature below the saturation temperature (~ 0 – 10°C) corresponding to the ESEM chamber vapor pressure of ~ 700 – 1300 Pa (~ 5 – 10 Torr). Stable droplet distribution is achieved according to the procedure developed by Stelmashenko *et al.*²³ The drops are imaged with a frame time of 1 s and corresponding images are captured with a 1 Hz frequency. As shown in Fig. 1(a), when imaged at low electron beam current and large viewing area, the drops can remain unchanged over relatively long time periods but evaporate relatively quickly (e.g., within 3 s) when imaged at higher current. In order to quantify the magnitude of the electron beam heating effects, the characteristic length, L^* , defined as four times the ratio of the drop area divided by the perimeter, was evaluated for each captured image. Figure 1(b) shows the time evolution of L^* corresponding to the images shown in Fig. 1(a). For all imaging settings, the decrease in L^* was linear in time (i.e., dL^*/dt was constant—see Fig. 1(b), for example). This fact allows for the use of calculated dL^*/dt as a criterion for comparison of the electron beam heating effect at different beam energies and currents. As demonstrated in Fig. 1(c), the experimental results

^{a)}Electronic mail: konrad.rykaczewski@nist.gov.

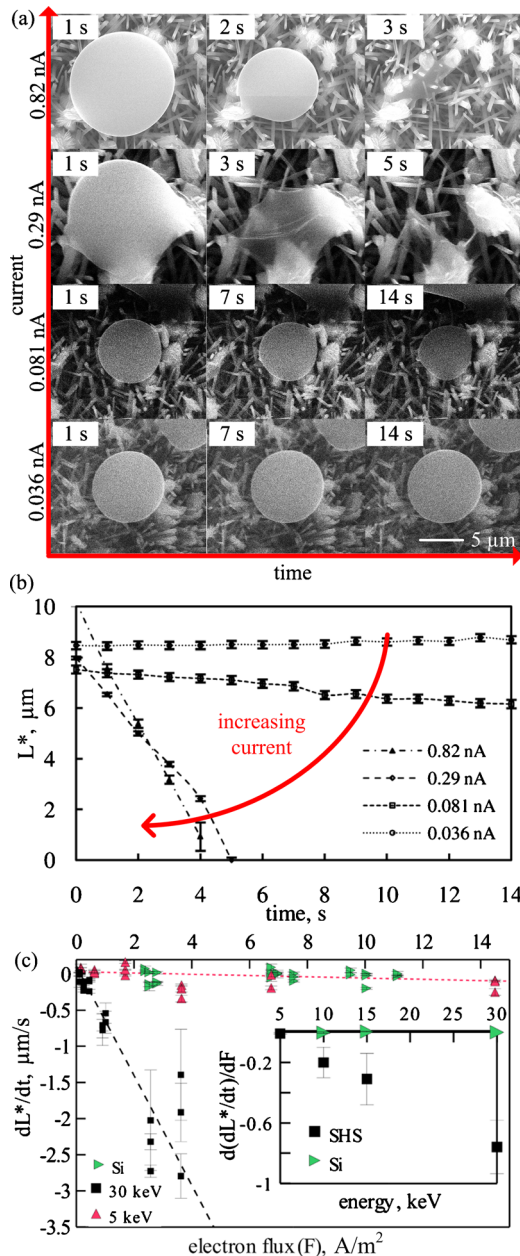


FIG. 1. (Color online) (a) 20° tilt images of water drops captured with a frequency of 1 Hz during ESEM imaging on SHS at 930 Pa, 5 °C, 6.2 mm working distance, 18.6 × 17.1 μm² viewing area, and electron beam energy of 30 keV, and varied currents, (b) corresponding plot of drop characteristic length, L^* , vs time, (c) the rate of change in the characteristic length, dL^*/dt , as a function of electron flux F (electron beam current divided by viewing area) for drops on a SHS at 20° tilt for electron beam energies of 5 and 30 keV (10 and 15 keV on SHS are omitted for clarity) and on silicon surface at ~54° tilt for electron beam energies of 10, 15, and 30). The insert shows relation between the estimated rate of change in dL^*/dt with the electron flux [$d(dL^*/dt)/dF$] as a function of electron beam energy for SHS and silicon.

can be further generalized by plotting dL^*/dt against the electron flux, F , defined as the ratio of the electron beam current to the viewing area. As shown in Fig. 1(c), dL^*/dt increases with the electron beam flux. To better illustrate the relationship of dL^*/dt to electron beam energy, we assume a linear relationship between dL^*/dt and electron flux and plot the slope of the calculated fits [$d(dL^*/dt)/dF$] against electron beam energy. The increase in scatter of data for dL^*/dt above ~1.5 μm/s is an indication extreme heating resulting in comparable evaporation and scanning rates. As clearly

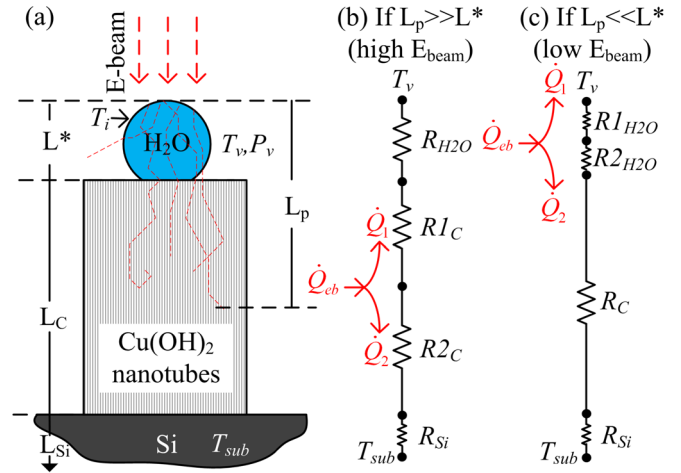


FIG. 2. (Color online) (a) Schematic of the physical arrangement in ESEM imaging of drops on a nanostructured SHS, (b) thermal resistance network for analyzing electron beam heating of a drop for $L_p \gg L^*$ case, and (c) for $L_p \ll L^*$ case.

shown in insert in Fig. 1(c), $d(dL^*/dt)/dF$ increases with energy for imaging of drops on the superhydrophobic. However, no decrease in L^* was observed for any imaging conditions of drops condensed on silicon surface. The details of the standard error and linear fitting calculations are described in Ref. 30.

To better understand the observed experimental trends we develop a simple model of the condensed droplet electron beam heating process.³⁰ As schematically shown in Fig. 2(a), we assume that most of the energy lost by the beam electrons, \dot{Q}_{eb} , is deposited within a short distance of the beam impact point, comparable to the penetration depth of the beam (L_p). The heat source term, \dot{Q}_{eb} , is assumed to be proportional to the product of the electron beam energy (E), current (i), one minus the backscatter electron coefficient ($1 - \eta_{BSE}$), projected area of the drop, and an area factor f taking into account the scan rate and viewing area. Using conservation of energy, we solve for the portion of the heat being conducted away through the liquid-vapor interface, \dot{Q}_1 , in terms of individual thermal resistances of the system components. Assuming that $\dot{Q}_1 = \dot{m}h_{lv}$, we can relate dL^*/dt to electron beam energy and current as well as material properties and dimensions:

$$\dot{Q}_1 = \dot{m}h_{lv} = \rho_l h_{lv} \frac{dV}{dt} = \rho_l h_{lv} \frac{\pi}{2} L^{*2} \frac{dL^*}{dt} \rightarrow \frac{dL^*}{dt} \sim \frac{iEf}{2\rho_l h_{lv}} (1 - \eta_{BSE}) \alpha, \quad (1)$$

where \dot{m} is the mass transfer rate across the interface, V is the drop volume, α is the ratio of the thermal resistance above which \dot{Q}_{eb} is generated and total thermal resistance, and h_{lv} and ρ_l are the latent heat of vaporization and density of water, respectively. As observed in the experiments, dL^*/dt increases with the electron beam current and energy. Since thermal resistance is proportional to the ratio of characteristic length divided by thermal conductivity of the material and cross sectional area, the relation in Eq. (1) also clearly explains the low evaporation rate observed for water drops condensed on a silicon substrate. While nearly inde-

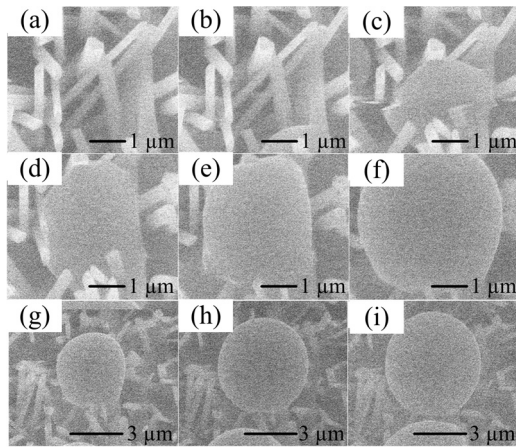


FIG. 3. ESEM imaging of subsequent steps of single water drop growth process with [(a)–(f)] $4.6 \times 4.3 \mu\text{m}^2$ and [(g)–(i)] $9.3 \times 8.5 \mu\text{m}^2$ viewing area imaged at 20° tilt with a frame frequency of 1 Hz on SHS at 930 Pa, 5°C , 6.2 mm working distance, and electron beam energy and current of 10 keV and 0.013 nA, respectively.

pendent of energy for a flat surface, the backscatter electron yield will significantly increase with decreasing energy for high contact angle (i.e., small surface footprint) drops of a few micrometer in diameters. This fact explains why imaging at lower beam energies with higher currents results in lower dL^*/dt than imaging at higher beam energies with lower current.

Direct quantification of electron beam heating effects at viewing fields smaller than $9.3 \times 8.5 \mu\text{m}^2$ is challenging due to difficulty in obtaining stable drops with diameters below $\sim 5 \mu\text{m}$. However, by fitting the relation between the dL^*/dt and the electron flux, we can estimate the evaporation rate occurring at a given electron beam energy, current, and viewing area. Based on our experimental results, an electron beam energy of 10 keV and low current (~ 0.013 nA) is an optimal compromise with acceptable image quality and minimal beam heating effects (imaging at electron beam energy below 10 keV and required working distances for 20° tilt results in poor imaging contrast). Imaging at these optimized conditions and viewing area of $4.6 \times 4.3 \mu\text{m}^2$ results in an estimated dL^*/dt of $-0.1 \mu\text{m/s}$ ($\sim 2\%$ of viewing field width per second) but doubling of the magnification to a corresponding viewing area of $2.3 \times 2.2 \mu\text{m}^2$ results in an unacceptably high estimated dL^*/dt of $-0.5 \mu\text{m/s}$ ($\sim 20\%$ of viewing field width per second). Thus, a viewing area of $4.6 \times 4.3 \mu\text{m}^2$ is the approximate limit for ESEM visualization of drops on the $\text{Cu}(\text{OH})_2$ SHS with negligible electron beam heating effects. As shown in Fig. 3, when imaged at these settings, vapor condensation initially proceeds through a combination of wetting and filling in the spaces between the $\text{Cu}(\text{OH})_2$ nanotubes until a liquid bridge is formed to a flat external surface with characteristic dimension of ~ 2 to $4 \mu\text{m}$. Subsequently, a liquid drop begins to emerge from the liquid spot with most of the growth due to significant contact angle increase with nearly constant base area where the droplet contacts the supporting surface. When enlarged to a diameter of ~ 4 – $6 \mu\text{m}$, the drop reaches a near spherical shape and switches from a near-constant-base area growth mode to a near-constant-contact angle mode. At this stage, the droplet grows until it coalesces with its neighbors.

In summary, in this work we quantify the electron beam heating induced evaporation rates of water drops on a SHS

for the range of beam settings available in a typical ESEM. The experimentally observed trends agree well with a single energy deposition/conduction model and underline the contribution of the high thermal resistance of the nanostructured layer to the high evaporation rates observed while imaging at higher magnification. We establish that at optimal ESEM imaging settings (10 keV and 0.013 nA), electron beam heating effects limit the viewing area to approximately $4.6 \times 4.3 \mu\text{m}^2$. When imaged using those settings, individual water droplet growth proceeds in three stages: (1) wetting and filling of an area with ~ 2 – $4 \mu\text{m}$ characteristic dimension between the nanotubes, (2) near constant base area growth until reaching emergence of a nearly spherical drop with dimension of ~ 4 – $6 \mu\text{m}$, and (3) constant contact angle growth until coalescence with other drops.

This research was performed while K.R. held at NRC ARRA fellowship at NIST and AGF was supported by AFOSR BIONIC Center under Award No. FA9550-09-1-0162. The authors acknowledge C. Dietz and Y. K. Joshi from Georgia Institute of Technology for providing samples of cupric hydroxide SHSs.

- ¹E. Schmidt, W. Schurig, and W. Sellschopp, *Forsch. Ingenieurwes.* **1**, 53 (1930).
- ²V. P. Carey, *Liquid-Vapor Phase-Change Phenomena*, 2nd ed. (Taylor and Francis, New York, 2008).
- ³K. K. S. Lau, J. Bico, K. B. K. Teo, M. Chowalla, G. A. J. Amarantunga, W. L. Milne, G. H. McKinley, and K. K. Gleason, *Nano Lett.* **3**, 1701 (2003).
- ⁴C. H. Chen, Q. J. Cai, C. L. Tsai, C. L. Chen, G. Y. Xiong, Y. Yu, and Z. F. Ren, *Appl. Phys. Lett.* **90**, 173108 (2007).
- ⁵J. B. Boreyko and C. H. Chen, *Phys. Rev. Lett.* **103**, 184501 (2009).
- ⁶X. M. Li, D. Reinhoudt, and M. Crego-Calama, *Chem. Soc. Rev.* **36**, 1350 (2007).
- ⁷C. Dorrer and J. Ruhe, *Soft Matter* **5**, 51 (2009).
- ⁸R. D. Narhe and D. A. Beysens, *Langmuir* **23**, 6486 (2007).
- ⁹M. Nosonovsky and B. Bhushan, *Nano Lett.* **7**, 2633 (2007).
- ¹⁰M. Nosonovsky and B. Bhushan, *Langmuir* **24**, 1525 (2008).
- ¹¹Y. M. Zheng, D. Han, J. Zhai, and L. Jiang, *Appl. Phys. Lett.* **92**, 084106 (2008).
- ¹²Y. C. Jung and B. Bhushan, *J. Microsc.* **229**, 127 (2008).
- ¹³Y. C. Jung and B. Bhushan, *ACS Nano* **3**, 4155 (2009).
- ¹⁴C. Dietz, K. Rykaczewski, A. G. Fedorov, and Y. Joshi, *Appl. Phys. Lett.* **97**, 033104 (2010).
- ¹⁵C. Graham and P. Griffith, *Int. J. Heat Mass Transfer* **16**, 337 (1973).
- ¹⁶J. W. Rose, *Int. J. Heat Mass Transfer* **10**, 755 (1967).
- ¹⁷L. Glicksma and A. W. Hunt, *Int. J. Heat Mass Transfer* **15**, 2251 (1972).
- ¹⁸C. P. Royall, B. L. Thiel, and A. M. Donald, *J. Microsc.* **204**, 185 (2001).
- ¹⁹D. Aronov, M. Molotskii, and G. Rosenman, *Phys. Rev. B* **76**, 035437 (2007).
- ²⁰D. Aronov, G. Rosenman, and Z. Barkay, *J. Appl. Phys.* **101**, 084901 (2007).
- ²¹R. G. Mathews, D. J. Stokes, B. L. Thiel, and A. M. Donald, in *Electron Microscopy and Analysis 1999*, edited by C. J. Kiely (IOP, Bristol, 1999), pp. 95–98.
- ²²D. J. Stokes, B. L. Thiel, and A. M. Donald, *Scanning* **22**, 357 (2000).
- ²³N. A. Stelmashenko, J. P. Craven, A. M. Donald, E. M. Terentjev, and B. L. Thiel, *J. Microsc.* **204**, 172 (2001).
- ²⁴A. Liukkonen, *Scanning* **19**, 411 (1997).
- ²⁵A. Lauri, I. Riipinen, J. A. Ketoja, H. Vehkamäki, and M. Kulmala, *Langmuir* **22**, 10061 (2006).
- ²⁶S. E. Kirk, J. N. Skepper, and A. M. Donald, *J. Microsc.* **233**, 205 (2009).
- ²⁷J. E. McGregor and A. M. Donald, *J. Microsc.* **239**, 135 (2010).
- ²⁸W. Zhang, X. Wen, and S. Yang, *Inorg. Chem.* **42**, 5005 (2003).
- ²⁹X. Chen, L. Kong, D. Dong, G. Yang, L. Yu, J. Chen, and P. Zhang, *Appl. Surf. Sci.* **255**, 4015 (2009).
- ³⁰See supplementary material at <http://dx.doi.org/10.1063/1.3560443> for details of the SHS fabrication, expanded discussion of the model derivation, and uncertainty and data fitting calculations.